Synthetic Metals 253 (2019) 34–39

Contents lists available at ScienceDirect

Synthetic Metals

journal homepage: www.elsevier.com/locate/synmet

Polaron properties in pentathienoacene crystals

Marcelo Lopes Pereira Junior[a], Rayane Tayná da Costa Torres[b], Bernhard Georg Enders[b], Wiliam Ferreira da Cunha[a], Rafael Timoteo de Sousa Júnior[c], Luiz Antonio Ribeiro Júnior[a,b,*]

[a] Institute of Physics, University of Brasília, Brasília 70919-970, Brazil
[b] University of Brasília, PPG-CIMA, Campus Planaltina, 73345-010, Brasília, DF, Brazil
[c] Department of Electrical Engineering, University of Brasília, Brasília 70919-970, Brazil

ARTICLE INFO

Keywords:
Pentathienoacene
Charge transport
Polaron properties
Organic molecular crystals

ABSTRACT

A two-dimensional tight-binding model is used to study static and dynamical properties of polarons in pentathienoacene crystals. Our computational approach determines the spacial parameter to obtain stable polarons in these materials by using a version of the Holstein–Peierls Hamiltonian. The model takes intra and intermolecular electron-lattice interactions into account. Remarkably, the results show that the charge transport mechanism is essentially one-dimensional in pentathienoacene crystals. This property is due to the nature of the polaron localization. Moreover, we show that the polaron dynamics can occur for an electric field threshold that overcomes the standard value of organic crystalline semiconductors.

1. Introduction

Organic semiconductors are promising materials in manufacturing optoelectronic devices since they present several advantages when compared to their inorganic counterparts. This make the former particularly interesting materials for the electronics industry [1]. Essential features such as low environmental impact, recyclability, and low energy consumption for operation together with the high level of versatility presented by these materials makes them desirable sources for optoelectronic devices. Furthermore, their small thickness, flexibility, and transparency stand out when it comes to the fabrication of new green energy devices [2–6]. In their working principle, the charge transport mechanism plays a fundamental role and should be detailed understood to increase the system's efficiency.

Organic crystals present particularities for the charge transport mechanism that differ from other classes of semiconducting materials substantially, since they exhibit two types of electron-lattice (e-l) couplings: a local intramolecular, Holstein-type [7,8] and a non-local intermolecular Peierls-type [9]. The most studied molecular crystals in the literature regarding the charge transport traits are the oligoacenes such as anthracene, pentacene, and rubrene [10–18]. Oligothienoacenes — molecules formed by the fusion of thiophene rings —, in turn, have received less attention [19–21], although they do present interesting optoelectronic properties such as good efficiency for the transport of electrons and holes. Importantly, in-depth knowledge concerning the static and dynamical properties of charge carriers in these materials, although crucial to increase the performance of oligothienoacene-based systems, is still missing in the literature.

Herein, we investigate the stability and dynamics of polarons as charge carriers in pentathienoacene crystals. By using a two-dimensional tight-binding model, we examine the influence of both intra and intermolecular e–l couplings on their ground state geometries in the presence of an additional charge. Subsequently, we address the impact of an applied external electric field on the charge carrier dynamics in these materials. Our numerical approach gives essential information about the polaron's localization and the charge transport dimensionality in pentathienoacenes.

2. Methodology

The theoretical approach used here consists of a semi-classical Holstein–Peierls model that takes into account both intra and intermolecular electron-lattice interactions to describe two-dimensional organic molecular crystals. In this context, each lattice site represents a i, j pentathienoacene molecule where i and j index the lattice line and column, respectively (see Fig. 1). Here, three degrees of freedom are taken into account for each site of the lattice: $u_{i,j}$ represents the intramolecular distortions and $v_{i,j}^{x,y}$ represents the relative displacement of a molecule from its equilibrium position in x and y directions. It is worthwhile to mention that a two-dimensional model to treat organic molecular crystals is a fair approximation to the actual system, since these materials present strong in-plane electronic overlap and weaker

* Corresponding author.
E-mail address: ribeirojr@unb.br (L.A. Ribeiro Júnior).

https://doi.org/10.1016/j.synthmet.2019.04.016
Received 15 January 2019; Received in revised form 15 April 2019; Accepted 15 April 2019
Available online 06 May 2019
0379-6779/

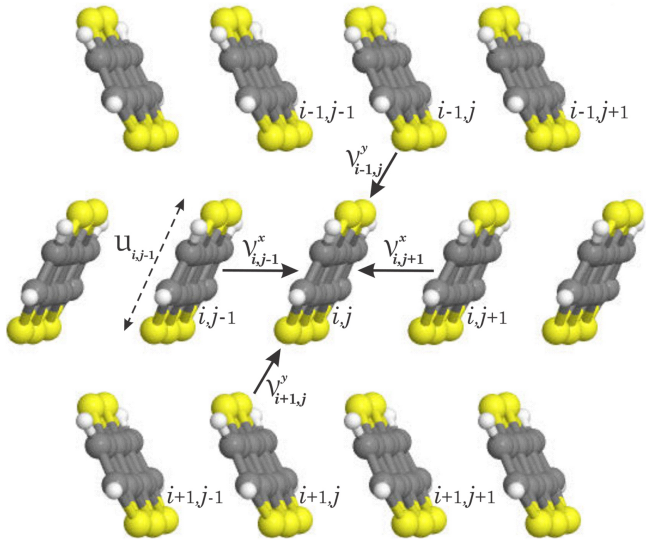

Fig. 1. Schematic representation of the herringbone arrangement for a pentathienoacene crystal. $u_{i,j}$ represents the intramolecular distortions and $v_{i,j}^{x,y}$ represents the relative displacements of each molecule in the x and y directions.

overlap between perpendicular molecular planes.

Based on the system's representation discussed above, our model Hamiltonian has the following form:

$$H = H_{e,1} + H_{e,2} + H_{l,1} + H_{l,2}, \tag{1}$$

where

$$H_{e,1} = \sum_{i,j} \alpha_1 u_{i,j} \hat{c}_{i,j}^{\dagger} \hat{c}_{i,j} \tag{2}$$

and

$$H_{e,2} = \sum_{i,j} (J_{i,j;\ i,j+1}^{x} \hat{c}_{i,j+1}^{\dagger} \hat{c}_{i,j} + \text{H. C.}) + \sum_{i,j} (J_{i,j;\ i+1,j}^{y} \hat{c}_{i+1,j}^{\dagger} \hat{c}_{i,j} + \text{H. C.}), \tag{3}$$

with

$$J_{i,j;\ i,j+1}^{x} = J_0^{x} - \alpha_2 (v_{i,j+1}^{x} - v_{i,j}^{x}) e^{i\gamma \Lambda_x(t)} \tag{4}$$

and

$$J_{i,j;\ i+1,j}^{y} = J_0^{y} - \alpha_2 (v_{i+1,j}^{y} - v_{i,j}^{y}). \tag{5}$$

In the equations above, J_0^{x} and J_0^{y} represent the transfer integrals in ordered system, when the sites are equally spaced. $\hat{c}_{i,j}^{\dagger}$ ($\hat{c}_{i,j}$) creates (annihilates) an electron at the (i, j)-site of the molecular matrix. α_1 (α_2) is the intramolecular (intermolecular) electron-phonon coupling. The electric field is assumed to be constant and is included, in Eq. (4), by using a time-dependent vector potential $\Lambda_x(t) = -cE_0 t$, in which c is the speed of light, E_0 is the uniform field strength. $\gamma = ea/\hbar c$, with e being the absolute value of the electronic charge and a the lattice constant. The usage of the time-dependent vector potential is a common strategy to allow the periodic boundary conditions for the action of the electric field, where the exponential comes from the Peierls substitution method [22].

For the lattice contribution, in turn, we consider intra and intermolecular harmonic oscillators as follows

$$H_{l,1} = \frac{K_1}{2} \sum_{i,j} (u_{i,j})^2 + \frac{M_1}{2} \sum_{i,j} (\dot{u}_{i,j})^2 \tag{6}$$

and

$$H_{l,2} = \frac{K_2}{2} \sum_{i,j} [(v_{i,j+1}^{x} - v_{i,j}^{x})^2 + (v_{i+1,j}^{y} - v_{i,j}^{y} r)^2] + \frac{M_2}{2} \sum_{i,j} [(\dot{v}_{i,j}^{x})^2 + (\dot{v}_{i,j}^{y})^2], \tag{7}$$

where K_1 and K_2 are the force constants and M_1 and M_2 are the harmonic oscillator masses. In these equations, the index 1 and 2 refer to intra and intermolecular modes, respectively.

Note that Eqs. (4) and (5) refer to the inclusion of the electron–phonon interactions. These equations form the basis of the well known Su–Schrieffer–Heeger (SSH) Hamiltonian [23,24]. The first term (J_0) defines the lowest order hopping integral. The second assumption provides the first-order correction to the hopping integral. This term couples the electronic states to the molecular geometry establishing the electron–phonon interaction, where α is the electron-phonon coupling constant. We employ these equations to consider lattice relaxation effects. Eqs. (6) and (7), in turn, refer to the intra and intermolecular lattice vibrations. In both equations, the first term denotes the harmonic "spring constant" which represents the increase in potential energy that results from the intramolecular displacements of the uniform sigma bonds (Equation (6)) and the intermolecular displacements imposed by the Van der Walls interactions (Eq. (7)). The second contribution stands for the kinetic energy of molecules. The SSH and the Holstein–Peierls Hamiltonians were broadly used, respectively, to study the polaron properties in conjugated polymers [25–30] and molecular crystals [31–36].

The time evolution of the system is carried out in the context of the Ehrenfest Molecular Dynamics [37]. Therefore, the electronic dynamics is described by the time-dependent Schrödinger equation (TDSE)

$$i\hbar \dot{\psi}(i, j, t) = H_{i,j;\ i',j'}(t) \psi_{i',j'}(t). \tag{8}$$

By introducing instantaneous eigenstates, the solution of TDSE at each instant can be expressed in the form

$$\psi(i, j, t + \Delta t) = \sum_{l} \left[\sum_{i',j'} \phi_l^{*}(i', j') \psi(i', j', t) \right] \times e^{\delta} \phi_l(i, j), \tag{9}$$

with $\delta = -i\varepsilon_l \Delta t/\hbar$. $\phi_l(i, j)$ and ε_l are the instantaneous eigenfunctions and eigenvalues for the electronic part of the Hamiltonian at a given time t, respectively [38]. Newtonian equations of motion for the molecules in the molecular array govern the intramolecular displacements with

$$F_u \equiv M_1 \ddot{u}_{i,j}(t) = -K_1 u_{i,j}(t) - \frac{\alpha_1}{M_1} \rho_{i,j;\ i,j}(t), \tag{10}$$

and the intermolecular displacements

$$\begin{aligned} F_{v^x} &= M_2 \ddot{v}_{i,j}^{x}(t) \\ &= -K_2 (2v_{i,j}^{x}(t) - v_{i,j+1}^{x}(t) - v_{i,j-1(t)}^{x}) \\ &- \frac{\alpha_2^{x}}{M_2} e^{-i\gamma A_x(t)} (\rho_{i,j;\ i,j-1}(t) - \rho_{i,j+1;\ i,j}(t)) \\ &- \frac{\alpha_2^{x}}{M_2} e^{i\gamma A_x(t)} (\rho_{i,j-1;\ i,j}(t) - \rho_{i,j;\ i,j+1}(t)), \end{aligned} \tag{11}$$

and,

$$\begin{aligned} F_{v^y} &= M_2 \ddot{v}_{i,j}^{y}(t) \\ &= -K_2 (2v_{i,j}^{y}(t) - v_{i+1,j}^{y}(t) - v_{i-1,j(t)}^{y}) \\ &- \frac{\alpha_2^{y}}{M_2} (\rho_{i,j;\ i-1,j}(t) - \rho_{i+1,j;\ i,j}(t)) \\ &- \frac{\alpha_2^{y}}{M_2} (\rho_{i-1,j;\ i,j}(t) - \rho_{i,j;\ i+1,j}(t)), \end{aligned} \tag{12}$$

where $\rho_{i,j;\ i',j'}(t)$ is the electron density matrix given by

$$\rho_{i,j;\ i',j'}(t) = \psi_{i,j}(t) \psi_{i',j'}^{*}(t). \tag{13}$$

The ground state lattice geometry is obtained from the resilient backpropagation (RPROP) algorithm [39] and later used in the dynamical calculations where the Euler-Lagrange equations are integrated over time using the Br”unger–Brooks–Karplus (BBK) integrator [40,41]. The set of parameters used in our simulations are presented in

Table 1
The set of model parameters used in the simulations performed here to describe a pentathienoacene lattice. Subscripts 1 and 2 refer to intramolecular and intermolecular modes, respectively. In the units below, "*as*" means attosecond.

Parameter	Symbol	Value
Lattice const.	a	3.5Å [20,19]
e–ph coupl. consts.	α_1, α_2	0.0–5.0 eV/Å [43]
Elect. field strength	E_0	0.2–3.2 mV/Å [10]
Transfer int. x-axis	J_0^x	173.0 meV [21,42,19]
Transfer int. y-axis	J_0^y	2.0 meV [21,42,19]
Spring const.	K_1	14.0 eV/Å^2 [43]
Spring const.	K_2	0.9 eV/Å^2 [43]
Oscillator mass	M_1	3.2×10^{10} eV(as/Å)^2
Oscillator mass	M_2	6.4×10^{10} eV(as/Å)^2

Table 1. These parameters were also used in other theoretical works and they show a good agreement with experimental estimates [21,20,19,42]. The strengths for the e-ph coupling constants vary within the interval established in Table 1 to investigate their impact on the formation and transport of polarons in model pentathienoacene crystals. The reference values for these parameters and for the spring constants are those used in the literature to model pentacene crystals in the context of a tight-biding approach [43]. The electric field strength lies in the regime used for time-of-flight mobility measurements in organic semiconductors [10]. The oscillator masses M_1 and M_2 are the mass of one and two pentathienoacene molecules, respectively, in units that are commonly used in SSH-based approaches. The transfer integrals, that account the electronic coupling between next-neighboring molecules, and the lattice parameter were derived from density functional theory (DFT) calculations by using the dimer-splitting method [19,21,42]. In all the cases studied here, we consider a two-dimensional 20×20 lattice and a simulation time of 5.0ps. Importantly, the Holstein–Peierls approach described above has been successfully used to study oligoacene crystals in previous researches, showing a good track record [33–35,31,32,43–46].

3. Results

In order to characterize the polaron's features in pentathienoacene crystals, we now discuss the results obtained for its ground state and dynamical properties, in which the latter is governed by the application of an external electric field. For the sake of convenience, we begin by discussing the ground state properties when polarons are formed. To do so, we use the inverse participation ration (IPR)

$$\mathrm{IPR} = \frac{\sum_{i,j} |\rho_{i,j}|^4}{\left(\sum_{i,j} |\rho_{i,j}|^2\right)^2}. \tag{14}$$

Here, the IPR defines a measurement of the polaron localization. In this perspective, for IPR values smaller than 0.3 the molecular charge spreads almost over all the lattice and no favorable charge localization to form stable polarons take place. On the other hand, IPR values greater than 0.8 denotes that the charge is localized almost entirely in a particular molecule. Such a localization trend is associated to the presence of a quasiparticle named small polaron. IPR values between 0.3 and 0.8 define the large polaron solutions, that are the most interesting quasiparticles when it comes to the charge transport description in organic crystalline semiconductors [47].

Based on this overview of the IPR measurement, Fig. 2 presents the impact of the interplay between the local and nonlocal e–ph couplings on the stability of polarons in our model pentathienoacene crystals.

From this figure, we can define four distinct regions representing different types of ground state solutions in the presence of an additional charge. Each of these areas correspond to charge distributions of rather different properties. The white area (small values of α_1 and α_2) shows

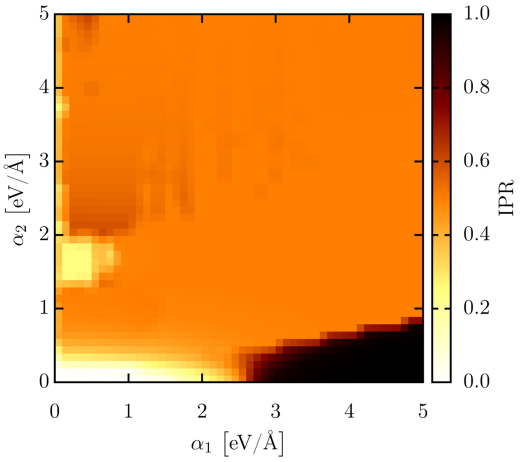

Fig. 2. Inverse participation ratio (IPR) as a function of the intra (local) and intermolecular (nonlocal) e–ph couplings.

IPR values close to zero, which indicates no polaron formation. This corresponds to delocalized solutions for the charge in the system. In this case, the charge transport mechanism is metallic-like, thus being mediated by free-like electrons [48]. For these e-ph coupling strengths, the charge weakly interacts with the lattice, and the particle can move almost freely through it. Another distinct region takes place for small values of α_1 and for α_2 ranging in the interval 1.5–2.0 eV/Å(yellow region). In this case, the e–ph couplings interplay yields a ground state solution of metastable polarons, i.e., a polaronic-like structure is formed by concentrating charge in four molecular units that are followed by respective lattice deformations. Such a quasiparticle solution, however, is not mobile in the presence of an external electric field, as revealed in our dynamics simulations (see Fig. 3). Therefore, this type of quasiparticle it is not relevant in describing the charge transport in the context of organic semiconductors. The orange area in Figure 2 displays IPR values between 0.3 and 0.8 that denote the most stable carrier structures with considerable local and nonlocal contributions for the charge localization that gives rise to large polaron solutions. For such a polaron configuration, the charge is essentially shared by five molecular units: a central one and its four immediate neighbors in the direction with higher strength of intermolecular transfer integral (see Fig. 3). Due to the high degree of anisotropy presented by pentathienoacene crystals, substantial part of the charge is distributed in a single molecular line following the direction of higher hopping parameter. Finally, for relatively low α_2 (< 2.0 eV/Å) and high α_1 (> 2.5 eV/Å), represented by the black area of Fig. 2, the additional charge is essentially localized in a single molecular unit (IPR > 0.8) thus yielding the small polaron solution (Holstein polaron [49,50]).

Our approach can also provide valuable information concerning the geometric configuration of the polaron. Fig. 3 depicts the molecular charge localization (black line) as well as the intramolecular displacements (red line) for a model pentathienoacene lattice containing an additional charge. In this figure, one can note that the mutual interaction between charge and lattice forms local lattice distortions in the region containing the excess charge. One molecule retains almost $0.5e$ of the charge whereas the two left and right next-neighboring ones symmetrically share the rest. Due to the presence of intramolecular electron-lattice interactions, the molecules are distorted (or compressed) in the presence of charge by following the profile of the charge distribution. Therefore, these molecular compressions are coupled to the net charge yielding a stable polaron.

Another important feature associated to the presence of polarons in organic crystalline semiconductors is the geometrical configuration of the intermolecular lattice distortions. These distortions contribute to defining the effective mass of the charge carrier [47,51]. When it comes to pentathienoacene crystals — due to their high degree of anisotropy

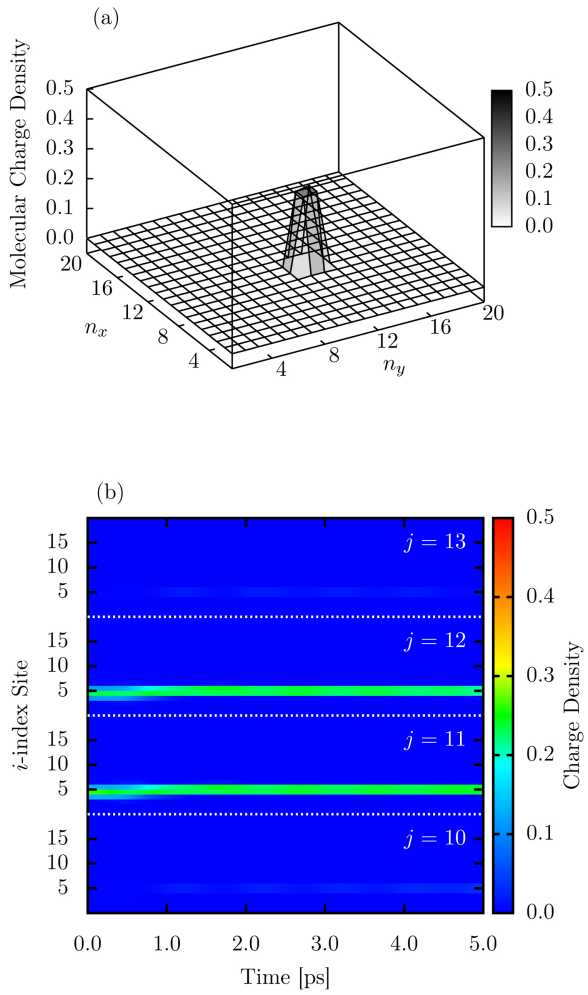

Fig. 3. (a) Ground state arrangement of the molecular charge density for a metastable polaron. (b) Time evolution of the molecular charge density for a metastable polaron. Panel (b) shows the two molecular lines containing the charge ($j = 11$ and $j = 12$) as well as two parallel lines ($j = 13$ and $j = 10$) above and below the region where the polaron is localized. One can note that the charge occupies the sites 5 and 6 in both $j = 11$ and $j = 12$ lines until the end of the simulations, for an electric field strength of 3.2 mV/Å. In this sense, no polaron motion is realized.

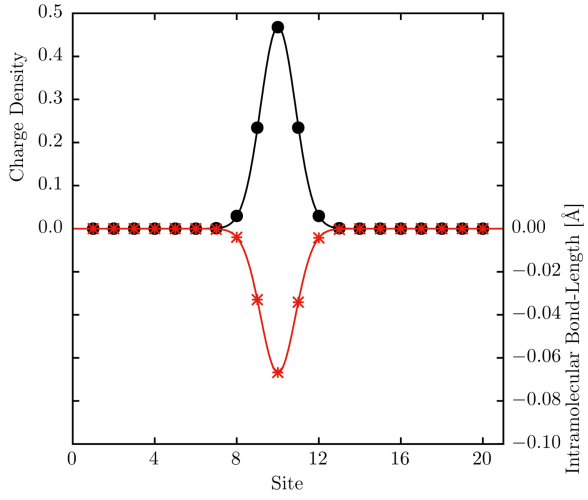

Fig. 4. Molecular charge density (black line) and intramolecular lattice distortions (red line). (For interpretation of the references to color in this figure legend, the reader is referred to the web version of this article.)

for the electronic hopping — the site displacements are primarily localized in the crystal's direction with higher strength for the intermolecular transfer integral. In this perspective, Fig. 4 shows the intermolecular displacements, in the x-direction, for different lines in the crystal (from line 09 up to line 13). Here, the polaron center is placed in the 11-th line of the lattice. The molecules in this line respond to the presence of the charge by displacing themselves from their equilibrium position, which polarizes a region of the crystal. A positive relative displacement for the sites in the left of the polaron center (site 210) can be observed since the molecules move from their equilibrium position towards the region where the charge is localized. Symmetrically, the sites in the right of the site 210 have a negative relative displacement, representing a shift to the left, towards the center of the polaron. These intermolecular bond expansions decrease by a δ/n_x factor, where δ is the value of the first positive bond-length ($v^x_{i+1,j} - v^x_{i,j}$) and n_x is the total number of molecules in the x-direction. This geometrical arrangement of the lattice in the presence of an additional charge is expected in the context of our model in order to maintain the constraint of the fixed total displacement, *i.e.*, $\sum_{i=1}^{n_x} (v^x_{i+1,j} - v^x_{i,j}) = 0$.

Finally, we discuss the features presented by the polaron dynamics in model pentathienoacene crystals. Due to the high anisotropy degree for the electronic coupling, the charge transport in pentathienoacene crystals is essentially one-dimensional and it takes place in the direction of highest coupling strength (x-direction in our model). Note that the external electric field acts only in the x-direction, according to Eq. (4). Since during the motion the polaron does not jump between parallel lines in the molecular matrix, its transport always occurs within the same line. Therefore, we use the equation below (Eq. (15)) to derive the molecular charge center for the line where the polaron lies initially. We have control for positioning the polaron at any part of the lattice in the ground state calculations. In this sense, here we analyze the influence of different intensities of an external electric field on the polaron transport, as illustrated in Fig. 5. Fig. 5(a) shows the time evolution of the molecular charge center, which is given by

$$\langle x_p(t)\rangle = \frac{n}{2\pi} \arg\left(\sum_{l=1}^{n} \exp\left(\frac{2\pi \mathrm{i}\, l}{n}\right)\bar{\rho}(t)\right) a, \tag{15}$$

where n is the total number of molecules and a is the lattice constant. For all field strengths, the polaron moves almost linearly by presenting similar saturation velocities. Importantly, these field strengths lie in the range of values usually adopted when it comes to organic materials [10]. The polaron transport mechanism can be understood by observing Fig. 5(b), that uses the IPR definition presented in the previous section.

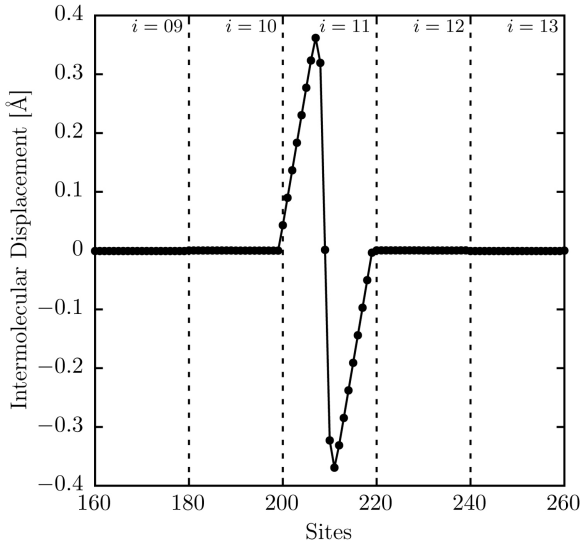

Fig. 5. Intermolecular displacements in the x-direction.

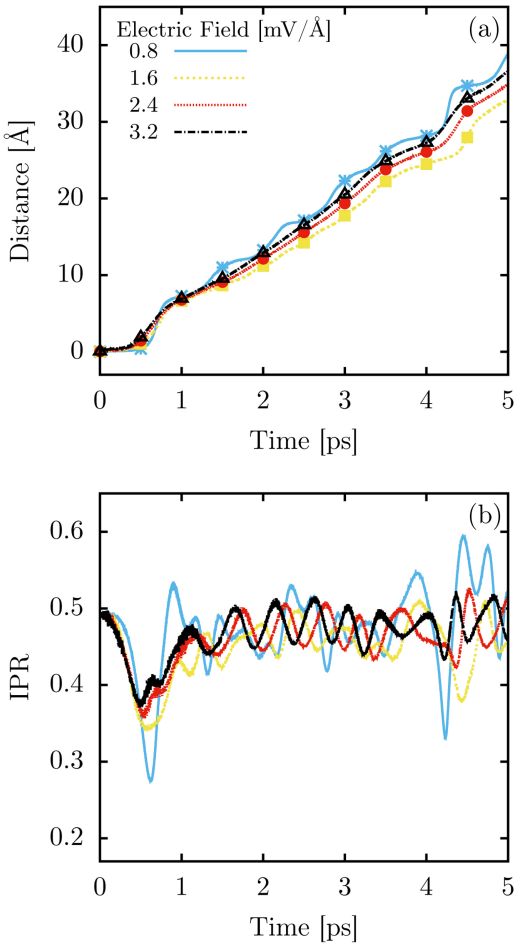

Fig. 6. Polaron dynamics for different electric field intensities. (a) Molecular charge center and (b) inverse participation ratio (IPR) as a function of time.

The first IPR values are referring to the standard polaron localization in the absence of an external electric field (note that all curves start from the same value, i.e., the IPR signature for the ground state polaron configuration). When the polaron initiates its motion, all molecular charge is shared between two molecules. This process initially decreases the IPR value to roughly 0.36. In the next step, most of the charge moves towards a central site rising the IPR value near to 0.5 again. This process continues until the end of the simulation by producing the oscillatory trend presented in Fig. 5(b).

Importantly, there are no implications associated to the oscillatory behavior of the IPR for the polaron dynamics as well as we believe that there is no overlap between the IPR measurement with other models that do not consider lattice relaxation effects explicitly. The IPR oscillations are consequence of the polaron transport mechanism in the scope of the Holstein–Peierls model. The polaron transference between neighboring molecules occurs into the following steps: most of the charge goes from being centered on a single molecule to being shared equally between two neighboring molecules and then drifts and gets centered on the next molecule. When the molecular charge is moving between the molecules, its center (or most of the charge) concentrates in two molecules. Since IPR is a measurement of the charge localization when the charge center is shared between neighboring molecules the IPR value decreases. After that, when the charge drifts and gets centered one molecule again, the IPR value increases. This process is repeated during the time yielding the oscillatory behavior of the IPR as shown in Figs. 5(b) and Fig. 6.

4. Conclusions

A semi-classical Holstein–Peierls model was used to study the polaron properties in pentathienoacene crystals. Our numerical approach is based on defining a parameter space in which stable polarons can be formed. Importantly, the interplay between the intra and intermolecular electron-lattice parameters can produce quasiparticles of distinct natures raging from free-like electrons to stable large polarons. The set of parameters that yields large polarons is the most interesting to describe the charge transport. Moreover, our results shown that in pentathienoacene crystals the polaron transport is essentially one-dimensional due to the high anisotropy degree presented by the electronic hopping parameters.

Acknowledgement

The authors gratefully acknowledge the financial support from Brazilian Research Councils CNPq and FAP-DF and CENAPAD-SP for providing the computational facilities. This research work has the support of the Brazilian Ministry of Planning, Development and Management (Grant 005/2016 DIPLA – Planning and Management Directorate). L.A.R.J., B.G.E.N, and W.F.C. gratefully acknowledge the financial support from FAP-DF grants 0193.001511/2017, 0193.001556/2017, 0193.001694/2017 respectively.

References

[1] J.M. Shaw, P.F. Seidler, Organic electronics: introduction, IBM J. Res. Dev. 45 (1) (2001) 3–9.
[2] A.M. Bagher, Comparison of organic solar cells and inorganic solar cells, Int. J. Renew. Sustain. Energy 3 (2014) 53–58.
[3] R. Friend, R. Gymer, A. Holmes, J. Burroughes, et al., Electroluminescence in conjugated polymers, Nature 397 (6715) (1999) 121.
[4] N. Greenham, S. Moratti, D. Bradley, R. Friend, A. Holmes, Efficient light-emitting diodes based on polymers with high electron affinities, Nature 365 (6447) (1993) 628–630.
[5] G. Li, V. Shrotriya, J. Huang, Y. Yao, T. Moriarty, K. Emery, Y. Yang, High-efficiency solution processable polymer photovoltaic cells by self-organization of polymer blends, Nat. Mater. 4 (11) (2005) 864.
[6] W. Ma, C. Yang, X. Gong, K. Lee, A.J. Heeger, Thermally stable, efficient polymer solar cells with nanoscale control of the interpenetrating network morphology, Adv. Funct. Mater. 15 (10) (2005) 1617–1622.
[7] T. Holstein, Studies of polaron motion: Part i. The molecular-crystal model, Ann. Phys. 8 (3) (1959) 325–342.
[8] T. Holstein, Studies of polaron motion: Part ii. The “small” polaron, Ann. Phys. 8 (3) (1959) 343–389.
[9] H. Fröhlich, Electrons in lattice fields, Adv. Phys. 3 (11) (1954) 325–361.
[10] V. Coropceanu, J. Cornil, D.A. da Silva Filho, Y. Olivier, R. Silbey, J.-L. Brédas, Charge transport in organic semiconductors, Chem. Rev. 107 (4) (2007) 926–952.
[11] S. Cho, E. Lim, Electrical and optical analyses of trapping phenomenon with temperature dependence of organic device, Org. Electron. 50 (2017) 397–402.
[12] L. Basiricò, A.F. Basile, P. Cosseddu, S. Gerardin, T. Cramer, M. Bagatin, A. Ciavatti, A. Paccagnella, A. Bonfiglio, B. Fraboni, Space environment effects on flexible, low-voltage organic thin film transistors, ACS Appl. Mater. Interfaces 9 (2017) 35150–35158.
[13] R.-R. Ji, Q. Wang, J.-X. Hu, S. Duhm, Impact of room temperature on pentacene thin film growth and electronic structure, Can. J. Chem. 95 (11) (2017) 1–5.
[14] J.E. Anthony, Functionalized acenes and heteroacenes for organic electronics, Chem. Rev. 106 (12) (2006) 5028–5048.
[15] C.D. Dimitrakopoulos, P.R. Malenfant, Organic thin film transistors for large area electronics, Adv. Mater. 14 (2) (2002) 99–117.
[16] T.W. Kelley, P.F. Baude, C. Gerlach, D.E. Ender, D. Muyres, M.A. Haase, D.E. Vogel, S.D. Theiss, Recent progress in organic electronics: materials, devices, and processes, Chem. Mater. 16 (23) (2004) 4413–4422.
[17] G. Horowitz, et al., Organic field-effect transistors, Adv. Mater. 10 (5) (1998) 365–377.
[18] J.E. Anthony, The larger acenes: versatile organic semiconductors, Angew. Chem. Int. Ed. 47 (3) (2008) 452–483.
[19] E.-G. Kim, V. Coropceanu, N.E. Gruhn, R.S. Sánchez-Carrera, R. Snoeberger, A.J. Matzger, J.-L. Brédas, Charge transport parameters of the pentathienoacene crystal, J. Am. Chem. Soc. 129 (43) (2007) 13072–13081.
[20] X. Zhang, X. Yang, H. Geng, G. Nan, X. Sun, J. Xi, X. Xu, Theoretical comparative studies on transport properties of pentacene, pentathienoacene, and 6,13-dichloropentacene, J. Comput. Chem. 36 (12) (2015) 891–900.
[21] K. Takimiya, M. Nakano, H. Sugino, I. Osaka, Design and elaboration of organic molecules for high field-effect-mobility semiconductors, Synth. Met. 217 (2016) 68–78.

[22] A.H. Castro Neto, F. Guinea, N.M.R. Peres, K.S. Novoselov, A.K. Geim, The electronic properties of graphene, Rev. Mod. Phys. 81 (2009) 109–162, https://doi.org/10.1103/RevModPhys.81.109.
[23] W.P. Su, J.R. Schrieffer, A.J. Heeger, Solitons in polyacetylene, Phys. Rev. Lett. 42 (1979) 1698–1701, https://doi.org/10.1103/PhysRevLett.42.1698.
[24] W.P. Su, J.R. Schrieffer, A.J. Heeger, Solitons excitations in polyeacetylene, Phys. Rev. B 22 (1980) 2099–2111, https://doi.org/10.1103/PhysRevB.22.2099.
[25] L.A. Ribeiro, P.H. Oliveira Neto, W.F. da Cunha, L.F. Roncaratti, R. Gargano, D.A. da Silva Filho, G.M. e Silva, Exciton dissociation and charge carrier recombination processes in organic semiconductors, J. Chem. Phys. 135 (22) (2011) 12B602.
[26] L.A. Ribeiro Junior, W.F. da Cunha, Nonadiabatic dynamics of injected holes in conjugated polymers, Phys. Chem. Chem. Phys. 19 (2017) 10000–10008.
[27] L.A. Ribeiro, W.F. da Cunha, P.H.O. Neto, R. Gargano, G.M. e Silva, Effects of temperature and electric field induced phase transitions on the dynamics of polarons and bipolarons, New J. Chem. 37 (2013) 2829–2836, https://doi.org/10.1039/C3NJ00602F.
[28] L.A. Riberio Junior, W.F. da Cunha, G.M. de Silva, Temperature effects on the scattering of polarons and bipolarons on organic conductors, J. Phys. Chem. A 118 (2014) 6272–6277, https://doi.org/10.1021/jp505590g.
[29] L.A.R. Junior, W.F. da Cunha, R. Gargano, G.M. e Silva, Singlet–singlet exciton recombination: theoretical insight into the influence of high density regime of excitons in conjugated polymers, J. Phys. Chem. B 118 (19) (2014) 5250–5257, https://doi.org/10.1021/jp4107926.
[30] L.A. Ribeiro, W.F. da Cunha, P.H.O. Neto, R. Gargano, G.M. e Silva, Impurity effects and temperature influence on the exciton dissociation dynamics in conjugated polymers, Chem. Phys. Lett. 580 (2013) 108–114, https://doi.org/10.1016/j.cplett.2013.06.065.
[31] E. Mozafari, S. Stafström, Polaron dynamics in a two-dimensional Holstein–Peierls system, J. Chem. Phys. 138 (18) (2013) 184104.
[32] E. Mozafari, S. Stafström, Polaron stability in molecular crystals, Phys. Lett. A 376 (22) (2012) 1807–1811.
[33] L.A.R. Junior, S. Stafström, Impact of the electron–phonon coupling symmetry on the polaron stability and mobility in organic molecular semiconductors, Phys. Chem. Chem. Phys. 18 (2016) 1386–1391, https://doi.org/10.1039/c5cp06577a.
[34] L.A.R. Junior, S. Stafström, Polaron stability in molecular semiconductors: theoretical insight into the impact of the temperature, electric field and the system dimensionality, Phys. Chem. Chem. Phys. 17 (14) (2015) 8973–8982.
[35] L.A.R. Junior, S. Stafström, Polaron dynamics in anisotropic Holstein–Peierls systems, Phys. Chem. Chem. Phys. 19 (5) (2017) 4078–4084.
[36] Z. Huang, M. Hoshina, H. Ishihara, Y. Zhao, Transient dynamics of super Bloch oscillations of a 1d Holstein polaron under the influence of an external ac electric field, Ann. Phys. 531 (1) (2019) 1800303.
[37] W.F. da Cunha, L.A.R. Junior, R. Garganoa, G.M. e Silva, Critical temperature and products of intrachain polaron recombination in conjugated polymers, Phys. Chem. Chem. Phys. 16 (2014) 17072–17080, https://doi.org/10.1039/c4cp02184c.
[38] Y. Ono, A. Terai, Motion of charged soliton in polyacetylene due to electric field, J. Phys. Soc. Jpn. 59 (8) (1990) 2893–2904.
[39] M. Riedmiller, H. Braun, A direct adaptive method for faster backpropagation learning: the Rprop algorithm, IEEE International Conference on Neural Networks, IEEE, 1993, pp. 586–591.
[40] A. Brünger, C.L. Brooks, M. Karplus, Stochastic boundary conditions for molecular dynamics simulations of ST2 water, Chem. Phys. Lett. 105 (5) (1984) 495–500.
[41] J.A. Izaguirre, D.P. Catarello, J.M. Wozniak, R.D. Skeel, Langevin stabilization of molecular dynamics, J. Chem. Phys. 114 (5) (2001) 2090–2098.
[42] J.-D. Huang, S.-H. Wen, K.-L. Han, First-principles investigation of the electronic and conducting properties of oligothienoacenes and their derivatives, Chemistry 7 (5) (2012) 1032–1040.
[43] M.L. Pereira Junior, R.T. de Sousa Junior, G.M. e Silva, L.A. Ribeiro Junior, Stationary polaron properties in organic crystalline semiconductors, Phys. Chem. Chem. Phys. 21 (2019) 2727–2733, https://doi.org/10.1039/C8CP06915H.
[44] M.L. Pereira, R.T. de Sousa, G.M. e Silva, L.A. Ribeiro, Modeling polaron diffusion in oligoacene-like crystals, J. Phys. Chem. C 123 (8) (2019) 4715–4720, https://doi.org/10.1021/acs.jpcc.8b11459.
[45] M.L.P. Junior, L.A.R. Junior, Polaron stability in oligoacene crystals, J. Mol. Model. 23 (2017) 89, https://doi.org/10.1007/s00894-017-3244-9.
[46] M.L.P. Junior, L.A.R. Junior, Polaron dynamics in oligoacene stacks, J. Mol. Model. 23 (2017) 257, https://doi.org/10.1007/s00894-017-3424-7.
[47] S. Stafström, Electron localization and the transition from adiabatic to nonadiabatic charge transport in organic conductors, Chem. Soc. Rev. 39 (2010) 2484–2499, https://doi.org/10.1039/b909058b.
[48] O. Ostroverkhova, Organic optoelectronic materials: mechanisms and applications, Chem. Rev. 117 (2016) 13279–13412, https://doi.org/10.1021/acs.chemrev.6b00127.
[49] T. Holstein, Studies of polaron motion: Part i. The molecular-crystal model, Ann. Phys. 8 (1959) 325–342, https://doi.org/10.1016/0003-4916(59)90002-8.
[50] T. Holstein, Studies of polaron motion: Part ii. The small-polaron, Ann. Phys. 8 (1959) 343–389, https://doi.org/10.1016/0003-4916(59)90003-X.
[51] A. Troisi, Charge transport in high mobility molecular semiconductors: classical models and new theories, Chem. Soc. Rev. 40 (2011) 2347–2358, https://doi.org/10.1039/c0cs00198h.